Cleaner and Circular Bioeconomy 1 (2022) 100005

Contents lists available at ScienceDirect

Cleaner and Circular Bioeconomy

journal homepage: www.elsevier.com/locate/clcb

A circular economy approach for phosphorus removal using algae biochar

Elsa Antunes[a,1,*], Arun K. Vuppaladadiyam[a,1], Ravinder Kumar[a], Varsha S.S. Vuppaladadiyam[b], Ajit Sarmah[c], Md Anwarul Islam[a], Tewodros Dada[a]

[a] College of Science and Engineering, James Cook University, Townsville, QLD 4811, Australia
[b] Department of Civil Engineering, AVN Institute of Engineering and Technology, Hyderabad, Telangana 501510, India
[c] Department of Civil and Environmental Engineering, The Faculty of Engineering, The University of Auckland, Private Bag 92019, Auckland 1142, New Zealand

ARTICLE INFO

Keywords:
Algae
Biochar
Circular economy
Phosphorus removal
Adsorption
Pyrolysis

ABSTRACT

In this study, a potential circular economy approach for macroalgae (*Ulva ohnoi*) was investigated considering the crucial stages of biorefinery. Important stages, such as drying of biomass, production of biochar (pyrolysis), and application of biochar for phosphorus removal were studied and reported. It is important to note that drying macroalgae biomass from an average wet basis moisture content of *ca.* 70–85% to a moisture content suitable for thermal conversion, *ca.* 10%, is a challenging task. The physicochemical properties of biomass as well as biochar were characterized and were correlated with their capacity to adsorb phosphorus (P). The initial thermal analysis of macroalgae biomass revealed that the major weight loss occurred between 150 and 550 °C. The kinetics of the pyrolysis process indicate the requirement of higher apparent activation energy in between 232 and 836 kJ mol^{-1}. An increase in the pore diameter, surface area, and pore volume in the biochar was noticed when the temperature of the pyrolysis process was increased. The highest P adsorption (78 mg-P/ g biochar) during the batch experiments was noticed with biochar obtained at 700 °C and can be due to the availability of alkali and alkaline earth metals. The kinetic study for P adsorption was described well by a pseudo second-order model. Biochar produced from macroalgae biomass can be considered as environmentally beneficial and low-cost adsorbent for phosphorus recovery. The biochar after adsorption may be used in agriculture as a slow release fertiliser due to significant amount of brushite.

1. Introduction

Circular economy (CE), owing to the negative impacts associated with a sustained growth in the consumption of finite fossil reserves, has received immense attention in the last few decades (Antunes et al., 2018b; Ubando et al., 2020). According to the Global Bioeconomy Summit, bioeconomy is "the knowledge-based production and utilization of biological resources, innovative biological processes and principles to sustainably provide goods and services across all economic sectors" (Birner, 2018). In short, CE can be viewed as the highly beneficial and a much needed shift from fossil based economy to a more dependable and sustainable bio-based economy (Nagarajan et al., 2013). CE emphasises on limiting the use of virgin resources and enhancing resource recovery and reuse (Ghisellini et al., 2016). Furthermore, CE has the potential to understand and implement new patterns that enable society to reach increased sustainability at low or no energy, material, and environmental cost (Ubando et al., 2020). As the CE focuses on a closed-loop approach in contrast to the linear approach, as observed in fossil based economy, it has the following added advantages: the possibility of carbon-neutral or -negative mode of biofuels production, greater environmental protection from non-degradable pollutants and elimination of secondary pollution (Nagarajan et al., 2013).

Modern agricultural practices are reliant on the widespread use of fertilizers, which result in an elevated concentration of phosphorus (P) in the run-off (Sun et al., 2018). P is an element that play a vital role in plant growth and used in fertilizers in the form of phosphates that are applied in large quantity to enhance crop yield. The unutilized P in the fertilizer is transported to the water bodies by the run-off water, causing eutrophication, which affects both the ecosystem and the economic progress (Veni et al., 2017). On the other side, the global demand for P has increased 1.9% between 2013 and 2018 and the reserves are expected to last for another 50 years, necessitating the reuse and recovery of this element (Novais et al., 2018). Studies conducted in the recent past have shown that P extraction from rock phosphate reserves and its use as fertilizer increased the accumulation of P in soil, *ca.* 6.9 ± 3.3 tetra gram-P/year (Yuan et al., 2018). It has also been reported by few authors that recovery of P from wastewater streams could reduce the P demand by 63% and categorised P in wastewater as a renewable phosphorus source (Nagarajan et al., 2020; Soltangheisi et al., 2019).

* Corresponding author.
E-mail address: elsa.antunes1@jcu.edu.au (E. Antunes).
[1] These authors contributed equally to this work.

https://doi.org/10.1016/j.clcb.2022.100005
Received 5 December 2021; Received in revised form 28 January 2022; Accepted 6 February 2022

Role of pyrolysis is critical and can be considered as one of the key processes in developing a circular economy to attain environmental sustainability. Pyrolysis, a thermochemical process, is carried out in an inert environment to produce liquid fuels, such as bio-oil (Dada et al., 2021). By closing the loops of previously used approach of linear processes, pyrolysis can tackle waste and energy challenges in a sustainable and circular mode (Antoniou et al., 2019). Biochar, one of the primary pyrolysis products, is a solid carbonaceous material possessing high carbon content amongst other several unique characteristics (Raheem et al., 2018). The effective utilization of biochar could significantly improve the economy of the pyrolysis process. Recently, biochars derived from marine macroalgae (MA) have gained increasing attention as a low-cost adsorbent for the removal of heavy metals and contaminants because MA is abundantly available. Further, biochar produced from MA holds high pollutant binding affinity as documented well in the literature (Jung et al., 2016; Kim et al., 2016). Noruzi et al. (2016) reported that biochar obtained from *Cladophora glomerata*, a green MA, had advantageous textural properties and chemical composition, such as uniformly distributed pores on the surface and availability of alkali and alkaline earth metals, making this biochar distinct from its counterparts (Norouzi et al., 2016). Subsequently, MA derived biochars exhibiting distinguished physicochemical characteristics have shown a great promise in the removal of a wide variety of pollutants from wastewater (Lucaci et al., 2019; Michalak et al., 2019). Evidently, several studies demonstrated that the biochar derived from marine and freshwater MA had higher pollutant removal efficiencies than those obtained from terrestrial biomass sources (Lucaci et al., 2019; Michalak et al., 2019). For instance, biochar produced from pyrolysis of *Laminaria japonica* and mixed with calcium alginate beads demonstrated the potential for P adsorption (Jung et al., 2016). Preliminary results revealed that pyrolysis at 600 °C produced the biochar with best physicochemical properties for P adsorption. Consequently, the biochar achieved a maximum P removal of nearly 97% and adsorption capacity of 157.70 mg/g. Kinetic and isothermal reports suggested that P adsorption onto biochar was an endothermic process, which is controlled by intraparticle diffusion rate and external mass transfer. Another study demonstrated the application of MA derived biochar for the adsorption of heavy metals and showed that the biochar achieved efficient heavy metal removal (Son et al., 2018). Noticeably, a maximum adsorption of 69.37 mg/g was obtained for copper by the biochar (Son et al., 2018).

As discussed above, biochar exhibits remarkable potential for heavy metal removal, encouraged by these findings the present study was designed to evaluate the potential of biochar derived from a MA (*Ulva ohnoi*) in removing phosphorus from an aqueous solution. Each biomass shows unique composition and the produced biochar at varying pyrolysis conditions could result in different physicochemical properties, consequently, may show interesting patterns for heavy metal adsorption. Hence, it is important to explore more biomass feedstocks to find biochar with efficient characteristics for heavy metals removal. In this regard, we performed pyrolysis of MA, varying the temperature from 300 to 800 °C, and observed the changes in physicochemical properties through various analytical techniques, and subsequently on P adsorption. Additionally, the batch experiments were conducted and adsorption kinetics were estimated to understand the adsorption behaviour of biochar. Finally, techno-economic analysis of biochar production was conducted to understand the feasibility of producing biochar from MA biomass.

2. Materials and methods

2.1. Biomass preparation and characterization

MA (*Ulva ohnoi*), was collected from Marine & Aquaculture Research Facilities Unit, James Cook University, Townsville, Northern Queensland, Australia. Before pyrolysis, the samples were dewatered through centrifugation at 300 rpm. At high temperatures, the colour of the algae deteriorates and proteins are susceptible to denaturation (Walker et al., 2020). Therefore, the temperature selected for drying was set at 60 °C. The dried biomass was then pelletised using a rotating pellet die to achieve a diameter of about 5 mm. The pelletising process increased the bulk density of the dried seaweed compared to its natural "flake" form or dry powder (2.1 g/cm^3). A thermogravimetric analyser (TA Instruments SDT-Q600) with simultaneous TG/DSC was used to examine the thermal behaviour of the MA sample. Biomass sample, with a *ca.* weight of 8 mg, was heated from room temperature to 1000 °C in a nitrogen environment at a flow rate of 50 mL min^{-1}. The experimental plan was designed for two stages. In stage I, a heating rate of 20 °C min^{-1} was used to understand weight loss pattern of the MA sample. In stage II, the tests were carried out using different heating rates, 20, 30 and 40 °C min^{-1}, to evaluate the kinetics for the pyrolysis process. The proximate and ultimate analyses along with the structural analysis were performed for the MA sample. The proximate analysis was done using the thermogravimetric analyser (TA Instruments SDT-Q600 Simultaneous TG/DSC), Costech elemental analyser was used to detect C, H, N, and O fraction, while 5E-AS3200B Automatic Coulomb Sulphur Analyser was used to detect the S content in the feedstock.

2.2. Pyrolysis kinetics

During the process of pyrolysis, the rate of reaction can be defined as,

$$\frac{d\alpha}{dt} = k(T)f(\alpha) \tag{1}$$

where k(T) is the reaction rate constant, which is a function of temperature, α is the degree of conversion and can be defined as,

$$\alpha = \frac{m_0 - m_t}{m_0 - m_\infty} \tag{2}$$

Where, m_0 is the initial mass of MA, m_t is the residual mass at temperature t, and m_∞ is the residual mass at equilibrium.

According to the Arrhenius equation, the reaction rate constant is defined as,

$$k(T) = Ae^{\left[\frac{-E_\alpha}{RT}\right]} \tag{3}$$

where A, E_α, R and T are frequency factor (pre-exponential factor, s^{-1}), the apparent activation energy (kJ mol^{-1}), the universal gas constant (8.314 J mol^{-1} K^{-1}) and temperature (°K), respectively.

From Eqs. (1) and (3), the heterogeneous solid state reaction can be defined as Mishra and Bhaskar (2014),

$$\frac{d\alpha}{dt} = k(T)f(\alpha) = Ae^{\left[\frac{-E_\alpha}{RT}\right]}f(\alpha) \tag{4}$$

where f (α) indicates the reaction mechanism function and t indicates the time.

The Friedman equation can be obtained by taking the logarithm on both sides of the above equation and rearranging the terms (Friedman, 1964):

$$\ln\left(\frac{\mathrm{d}\alpha}{\mathrm{d}t}\right) = \ln\left[A(\alpha)f(\alpha)\right] - \frac{E_\mathrm{a}(\alpha)}{RT} \tag{5}$$

The heating rate (β), in a non-isothermal process, can be defined as,

$$\beta = \frac{dT}{dt} = \frac{dT}{d\alpha} \times \frac{d\alpha}{dt} \tag{6}$$

Form the Eqs. (1), (3) and (6),

$$\frac{d\alpha}{dT} = \frac{A}{\beta}e^{\left[\frac{-E_\alpha}{RT}\right]}f(\alpha) \tag{7}$$

Upon integrating the above Eqs. (7), (8) can be expressed as,

$$g(\alpha) = \int_0^\alpha \frac{d\alpha}{f(\alpha)} = \frac{A}{\beta}\int_{T_0}^{T} e^{\left[\frac{-E_\alpha}{RT}\right]}dT \tag{8}$$

Eq. (8) does not have an exact solution and so, needs approximation to solve it. Taking into consideration their good adaptability and validity,

isoconversional methods are highly recommended by the International Confederation for Thermal Analysis and Calorimetry (ICTAC) to determine the apparent activation energy (E_α) for solid-state processes. Thus, to determine the kinetic triplet, two isoconversional methods, Kissenger-Akira-Sunnose (KAS) method and Friedman method, were selected and the E_α obtained from Friedman method was used to evaluate the pre-exponential factor and reaction mechanism. The KAS method is as follows Akahira and Sunose (1971):

$$\ln\left[\frac{\beta}{T^2}\right] = \ln\left[\frac{AR}{E_\alpha g(\alpha)}\right] - \frac{E_\alpha}{RT} \tag{9}$$

2.3. Biochar production and characterization

The biochar was produced via pyrolysis of MA (*Ulva ohnoi*) in a tubular furnace (Termolab), which is shown in Fig. S1. Ceramic pots containing biomass samples were placed in a quartz tube with an internal diameter of 64 mm. The chamber was sealed on either side, with provisions to allow nitrogen gas flow into the pyrolysis chamber and a water trap to collect bio-oil and pyrolysis gases. As the quantification and characterization of bio-oil and pyrolysis gases were not within the scope of the present study, they were not recorded and reported. The pressure and temperature within the reactor were monitored by a pressure gauge and Eurotherm 3216 temperature programmer controller, respectively. The MA samples, each weighing *ca.* 8 g, were put in a ceramic pot and placed in the middle of the tubular furnace. The reactor was purged with 6 L min^{-1} of N gas and pressure inside the reactor was manually stabilized between −5 and 0 kPa. Considering a temperature heating rate of 10 °C min^{-1} and holding time of 1 h, the MA samples were heated at 300, 400, 500, 600, 700 and 800 °C. Upon the completion of pyrolysis, the biochars were allowed to cool overnight in a nitrogen environment. The charred solid samples (biochars) were collected and milled to reduce the particle size below 150 μm and used for characterization and in the subsequent experiments.

Similar procedures, used for the characterization of biomass, were used for the proximate and ultimate analyses of the biochar samples. The SEM was used to understand the morphology of the MA derived biochars (SEM, SU5000, Hitachi Co., Japan). The pore size and pore volume were determined via N_2 adsorption using Quantachrome Autosorb iQ3. The samples were sieved (150 μm), followed by degassing at 300 °C under vacuum for 4 h. BET model was used to estimate the specific surface area of the biochar material and BJH (Barret-Joyner-Halenda) model was used to determine the pore size distribution and total volume of pores. The phase purity of the biochar samples was determined with D2 Phaser Model manufactured by Bruker ASX.

2.4. Phosphorus removal experiments

Preliminary experiments were carried out with all biochars produced at different pyrolysis temperatures to determine which biochar exhibited the highest P adsorption capacity. For this purpose, a stock solution, with 500 mg L^{-1} of phosphorus (concentration commonly found in domestic wastewater treatment plants), was prepared by mixing KH_2PO_4 (potassium dihydrogen phosphate) in deionized water. The P-stock solution was then diluted according to the requirement. A 100 mL of KH_2PO_4 solution was added to *ca.* 0.3 g of biochar and the mixture was continuously shaken for 24 h at 22 °C. The mixture was then filtered using a 0.22 μm membrane filter. The phosphate concentration in the filtrate was analysed by using an inductively coupled plasma atomic emission spectrometer (ICP-AES-Varian Liberty Series II). The phosphorus removal efficiency was evaluated as the difference of the initial phosphorous and final phosphorous concentration. The P removal experiments were conducted in duplicates and the average values are presented.

2.5. Adsorption kinetics and isotherms

The adsorption kinetics for phosphate adsorption onto MA derived biochar were conducted at room temperature (22 °C ± 2) in digestion vessels (100 mL) containing P solution (500 mg L^{-1}, pH 4.5 ± 0.1) mixed with 0.3 g of biochar. A mechanical shaker was used to agitate the samples continuously at 350 rpm, following the protocol reported earlier (Antunes et al., 2018a). The mixtures were taken out at regular intervals and were filtered using a membrane filter, 0.22 μm size, (GE cellulose nylon membrane), to determine the phosphate concentration. The difference between initial and final concentration of phosphate was used to understand the amount of P adsorbed on to the sorbent. The adsorption kinetic models, such as first-order (Eq. (10)), second-order (Eq. (11)), intraparticle diffusion (Eq. (12)) and Elovich (Eq. (13)) models were used to understand the kinetics of the adsorption process (Antunes et al., 2017a; Kim et al., 2020b). The following linear form of the equations were used:

$$\ln\left(q_e - q_t\right) = \ln q_e - k_1 t \tag{10}$$

$$t/q_t = 1/\left(k_2 q_e^2\right) + t/q_e \tag{11}$$

$$q_t = k_{id}\, t^{1/2} + C \tag{12}$$

$$q_t = (1/b)\ln ab + (1/b)\ln t;\ t_0 = 1/ab \tag{13}$$

where q_t and q_e indicate the quantity of phosphorus (mg/g) adsorbed in time t and at equilibrium, respectively, k_1 (h^{-1}) and k_2 (g mg^{-1} h^{-1}) are the first-order and second-order rate constants, respectively. While the first-order model is based on the mononuclear adsorption mechanism the second-order models are based on binuclear adsorption mechanisms. For the intraparticle diffusion model, k_{id} (g mg^{-1} $h^{-1/2}$) is the intraparticle diffusion rate constant and C (mg g^{-1}) is a constant. The Elovich model contains two constants, a is the rate constant of chemical adsorption and b is the constant of surface coverage (Kim et al., 2020b).

Adsorption isotherms of phosphate (300, 400, 500, 600, 800 and 1000 mg L^{-1}) on biochar were evaluated by mixing 0.3 g of biochar with 100 mL of P solution with varying concentrations in digestion vessels. The digestion containers were placed in a mechanical shaker and shaken at room temperature continuously for 24 h. Following similar procedure explained above, at regular intervals, all the samples were taken out and filtered for further analysis. Experiments were done in duplicates and average values were reported. The experimental data was simulated using Langmuir and Freundlich isotherm models using the following equations:

$$Langmuir\ \text{model}:\ q_e = KQC_e/\left(1 + KC_e\right) \tag{14}$$

$$Freundlich\ \text{model}:\ q_e = K_f C_e^n \tag{15}$$

where K (L mg^{-1}) and K_f ($mg^{(1-n)}L^n$ g^{-1}) are the Langmuir bonding term related to binding energies and Freundlich sorption coefficient, respectively. Q (mg g^{-1}) refers to the Langmuir maximum capacity, C_e (mg L^{-1}) is the solution concentration of the sorbate at equilibrium, and n is the Freundlich exponent that determines the degree of linearity.

2.6. Techno-economic analysis

The cost for biochar production was estimated based on previous studies, considering pilot plant cost of USD 120,000 (Feizi et al., 2020; Islam et al., 2011). Other parameters such as fixed capital investment (FCI), total Capital Requirement (TCR), annualised capital cost (ACC) were taken from the previous study (Feizi et al., 2020). Current wage rate in Australia is USD 15.26/h. Total annual salary of employees were calculated considering six shift operators working in the pilot plant. The feedstock cost of USD 28/tonne was reported in the literature for

macroalgae (dry basis) (Konda et al., 2015). Other parameters included in the techno-economic analysis are given in Table 4.

3. Results and discussion

3.1. Biomass characterization

The proximate and ultimate analyses, along with the biochemical analysis were performed for the selected MA (*Ulva ohnoi*) and the results are presented in Table S1. The MA had high ash content, *ca.* 31% by dry weight. Also, the biochemical analysis indicates that MA contains high proportions of carbohydrates followed by proteins and lipids. The thermogravimetric (TG) and derivative thermogravimetric (DTG) curves for MA sample are presented in Fig. S2. To understand the pyrolysis characteristics of algae biomass, it is important to understand the thermal behaviour of its major compositions of macroalgae, which are lipids, proteins and carbohydrates. Thus, the TG and DTG curves at a heating rate of 20 °C min^{-1} were considered to understand the thermal behaviour of the selected MA (*Ulva ohnoi*). The mass loss pattern of MA, noticed in this study, corresponds to those reported in earlier studies (Vuppaladadiyam et al., 2019a, 2019b; Zhao et al., 2019).

The DTG curve presented in Fig. S2(b) can be characterized into three stages. The weight loss in the first stage within the range 50–150 °C can be related to the elimination of lightweight hydrocarbons and water molecules (Hu et al., 2015). The weight loss in this stage was *ca.* 15%, indicating the presence of high water content. One plausible reason could be the long-term storage of the sample in the form of pellets. The second stage, between 150 and 550 °C, can be considered as the main pyrolysis or devolatilization zone, with the weight loss of *ca.* 40%. It is to be noted that major pyrolysis reactions such as cracking, decarboxylation and depolymerization reactions take place in this stage (Söyler et al., 2017). The DTG curve in the second stage can be characterised by a single peak followed by a shoulder on the right side. The maximum peak value 210 °C can be related to the degradation of proteins and carbohydrates (Dandurand et al., 2014). It should be noted that the peaks of carbohydrates and proteins, in general, overlap each other (Chen et al., 2014). A shoulder can be observed on the right side following the main peak, in the temperature range of 250–350 °C, which can be due to the degradation of lipids (Muniz et al., 2015). In the third stage, from 550 to 850 °C, a separate peak was found at *ca.* 720 °C, and the weight-loss can be related to the calcination of mineral contents together with the loss of carbonaceous matter (Wnetrzak et al., 2013). Similar TGA patterns were reported in previous studies carried out using algae like *Polysiphonia elongata* (Ceylan et al., 2014), *Chlorella vulgaris* ESP-31 (Bach and Chen, 2017) and *Nannochloropsis oculata* (Ceylan and Kazan, 2015).

3.2. Drying kinetics

In view of the challenges associated with the biofuel production from wet algae via any conversion process, drying of the produced biomass is an important and critical step; however, this aspect has not been fully investigated (Hosseinizand et al., 2018). Macroalgae has a significant amount of moisture content, *ca.* 80% wet basis, and it is often a challenging task to get such high moisture content to *ca.* 10%, which is suitable for thermal conversion. The process of drying is energy intensive and the lack of knowledge in the field of drying made the large-scale algae biorefinery concept economically unfeasible. Therefore, drying is a key process that needs to be studied to understand the cost-effectiveness of macroalgae pyrolysis. In the previous study, the drying kinetics of MA (*Ulva ohnoi*) showed that temperature and relative humidity are the key determinants for achieving an equilibrium moisture level in the biomass. Macroalgae have high equilibrium moisture, 10–60%db (at 45 °C and 10–50% relative humidity), which indicates that the double layers thick cells orientation of macroalgae hold extra moisture (Walker et al., 2020).

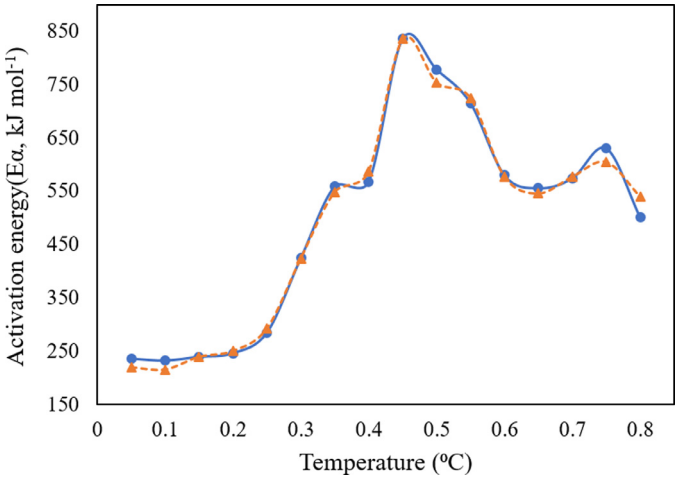

Fig. 1. Variation of activation energy for both Friedman and KAS methods, with respect to conversion for MA *Ulva ohnoi*.

On the contrary, effective diffusivity of macroalgae for radiative heating and convective heating were 3.2–8.8 × 10^{-8} and 1.2–1.5 × 10^{-7} m^2/s (at 40 – 60 °C), respectively. These values are significantly higher than other biomaterials such as wood, fruit slices (Walker et al., 2020). This finding demonstrates that MA exhibited a larger contact surface area for drying and thereby higher drying rate. However, convective heating assisted drying was more favourable than radiative heating. The drying of macroalgae is a substantial barrier to the economic feasibility of biorefinery or any macroalgae processing industry. To overcome this hurdle, several alternatives have been found in the literature. For instance, Vortex fluidic device (VFD) supported direct transesterification technique was successfully applied to produce biodiesel from wet microalgae biomass (Sitepu et al., 2018a, 2018b). This VFD process eliminated the drying step from the biodiesel production process. However, solar drying demonstrated significant success in MA drying which is a cost-effective and zero carbon footprint drying process for the tropical region (Fudholi et al., 2011; Hammond et al., 2018). Similarly, solar conductive drying of macroalgae recorded effective diffusivity of 1.355 × 10^{-7} m^2/s, which was much higher than the drying of macroalgae under vacuum (30 mbar at 60 °C) that provided an effective diffusivity of 9.451 × 10^{-8} m^2/s (Bheda et al., 2018). Drying, pyrolysis, and combined cycle power generation technology thus can be used as an alternative to reduce the overall energy consumption in bulk scale energy harvesting from macroalgae (Aziz et al., 2014). However, detailed cost analysis for drying of MA is still an unexplored topic, hence, could be an interesting and valuable analysis to perform in the near future.

3.3. Kinetic analysis based on TG

TG data, obtained for three heating rates, 20, 30 and 40 °C min^{-1}, was considered to assess the kinetics of the pyrolysis process. By using Eqs. (5) and (9), the apparent activation energies (E_α) were derived. The variation in E_α on conversion (α) is shown in Fig. 1 and are tabulated in Table S2. From Fig. 1, E_α varied considerably with regard to α, implying the involvement of many reaction mechanisms during the pyrolysis of MA sample (Gai et al., 2013). An examination of the data from Table S2 shows that the maximum E_α values were obtained at conversions of 0.45 and 0.75, which fell within the range of 835.5–836.1 and 605.1–630.6 kJ mol^{-1}. The lowest E_α values were found to be at conversions of 0.05–0.1, which could be likely due to the transition from dehydration to volatilization of major constituents of algae biomass, which are lipids, proteins and carbohydrates (Zhao et al., 2019). The activation energy requirement is generally high in the main pyrolysis zone, between temperatures 150–600 °C, because of the decomposition of complex organic

Table 1
Physicochemical properties of biochars obtained at varying pyrolysis temperatures.

Parameters/ Sample	Units	Biochar					
Pyrolysis temperature	°C	300	400	500	600	700	800
Yield	%	60.4	49.7	43.9	40.3	30.5	29.4
Retention time	min	60	60	60	60	60	60
Surface area (BET)	m^2/g	1.8	3.1	6.1	32.4	89.1	178
Total pore volume	mm^3/g	14	26	37	68	69	82
Avg. pore diameter	nm	3.5	3.8	3.9	3.9	3.8	3.8
Carbon	wt.% wt.% wt.% wt.%	32.6	32.7	32.9	30.4	28.9	28.3
Nitrogen		5.0	4.3	3.6	3.2	3.1	3.0
Hydrogen		3.3	2.5	1.6	0.9	0.5	0.5
Oxygen		30.5	29.3	27.0	24.7	16.1	16.9
O/C ratio		0.94	0.90	0.92	0.81	0.56	0.60
H/C ratio		0.10	0.08	0.05	0.03	0.02	0.02
Ash elements	g/kg						
Ca		18.1	–	29.5	–	40.4	–
P		4.44	–	5.54	–	7.92	–
Na		26.4	–	36.0	–	47.7	–
Mg		51.3	–	66.5	–	88.9	–
K		32.9	–	48.4	–	66.5	–
Al		57.5	–	107	–	123	–
Fe		0.27	–	1.59	–	2.25	–

matter (Bach and Chen, 2017; Figueira et al., 2015; Sanchez-Silva et al., 2013). The range of activation energies obtained in this study corresponds to those available in the literature (Ceylan and Kazan, 2015; Figueira et al., 2015; Maurya et al., 2016; Zhao et al., 2019). Further, the values of correlation coefficient for all the conversions were found to be high, demonstrating the reliability of the calculations.

Using the E_α generated via Friedman method, compensation effect (described in Supplementary Information under methods section) was used to evaluate the reaction mechanism f(α) and frequency factor (A). The values of A in the selected range of conversion are presented in Table S2. The linear correlation between Arrhenius parameters is shown in Fig. S3 and compensation line for MA *Ulva ohnoi*, is as follows:

$$InA_i = 0.224E_{\alpha i} - 2.5152 \quad (16)$$

Substituting the values of $E_a(\alpha)$ from Table S3 into Eqs. (10) and (11) will give the values of A(α), listed in Table S2. The variation in A(α) over few orders of magnitude indicates its severe dependence on α. The f(α) can be obtained from Eq. (13) by using the A(α) values derived earlier. The reaction mechanism function for MA *Ulva ohnoi*, presented in Fig. S3, was a rising function for α<0.15, declining function for 0.15>α<0.3. The reaction mechanism function for α<0.15 indicates acceleratory type functions, which corresponds to Avrami-Erofeev and power law models. A declining trend followed by an acceleratory phase is a typical characteristic of Avrami-Erofeev models, indicating the nucleation and nuclei growth process (Khawam and Flanagan, 2006). For α in between 0.3–0.35, the mechanism function displayed an acceleratory trend with respect to alpha. The f(α) declined continuously in the later stages, which could be related to order-based models, either diffusion or contracting models (Zhao et al., 2019).

3.4. Biochar production and characterization

The pyrolysis temperature significantly influences the biochar production and evidently, researchers noticed a decrease in biochar yields when the process temperature increases (Giwa et al., 2020). As shown in Table 1, biochar yields obtained in the present study were 60.4, 49.7, 43.9, 40.3, 30.5 and 29.4% at temperatures 300, 400, 500, 600, 700 and 800 °C, respectively. It is evident from previous studies that higher temperatures significantly promote secondary cracking reactions and deoxygenation reactions. As a result, a dominant portion of the feedstock is converted into gases, leaving behind less amount of char, thereby, producing lower biochar yields (Giwa et al., 2020). These findings correspond to the earlier demonstrations that displayed a comparable trend in biochar yields with increase in pyrolysis temperature (Colantoni et al., 2016; Zhang et al., 2016).

The textural and other physicochemical properties of the biochar are presented in Table 1. From this table, it is evident that surface area (SA) of biochar samples increased consistently with respect to pyrolysis temperature. Noticeably, 800 °C produced the biochar with highest SA of 178 m^2/g and 300 °C produced biochar with lowest SA of 1.8 m^2/g. Similarly, the total pore volume (TPV) in biochar also increased with the rise in pyrolysis process temperature. A possible reason for the increase in SA and TPV could be the release of elements or volatilization of biomass components into gases at high temperatures that probably created more adsorption sites for N_2 molecules for the analysis.

Elemental composition of biochars showed substantial changes with rise in temperature. It was noticed that C content in the biochar slightly increased with temperature till 500 °C and then decreased gradually, corresponding to the studies mentioned in the literature (Choi and Kan, 2019; Kim et al., 2020a, 2012). Additionally, from Table 1, with the rise in temperature, the H and O content in the biochar was noticed to decrease and this eventually led to the decrease in the H/C and O/C, suggesting a high hydrophobicity, carbonization and aromaticity (Table 1). A plausible explanation for this could be the increase in the degree of carbonization and reduction of polar functional groups on the biochar surface (Choi and Kan, 2019; Zheng et al., 2013). The content of metals in the ash increased with rise in the temperature (Table 1) and could significantly affect the adsorption of P.

Fig. S4 shows SEM images of MA (*Ulva ohnoi*) before pyrolysis and biochar samples obtained at temperatures of 300, 500, and 700 °C. The MA biomass has a smoth texture while the MA derived biochar shows a coarser surface that is highly porous. As can be observed in the SEM images, the thermal decomposition of the MA biomass leads to the production of biochar that is characterised by a rugged and irregular surface. SEM micrographs revealed noticeable changes in morphological structure with biochar at high temperature showing distinct porous nature as contrast to the sole biomass or biochar obtained at low temperatures. A visual examination of SEM images further suggests that there are mineral deposits on the biochar at elevated temperatures. SEM results are consistent with BET results that indicated the availability of higher amount of pores in the biochar produced at higher temperatures.

XRD patterns for sole biomass and produced biochars are shown Fig. 2. The results revealed that the biomass does not possess a crystalline structure. However, the biochar samples resulting from pyrolysis of MA at different temperatures exhibited sharp XRD peaks at

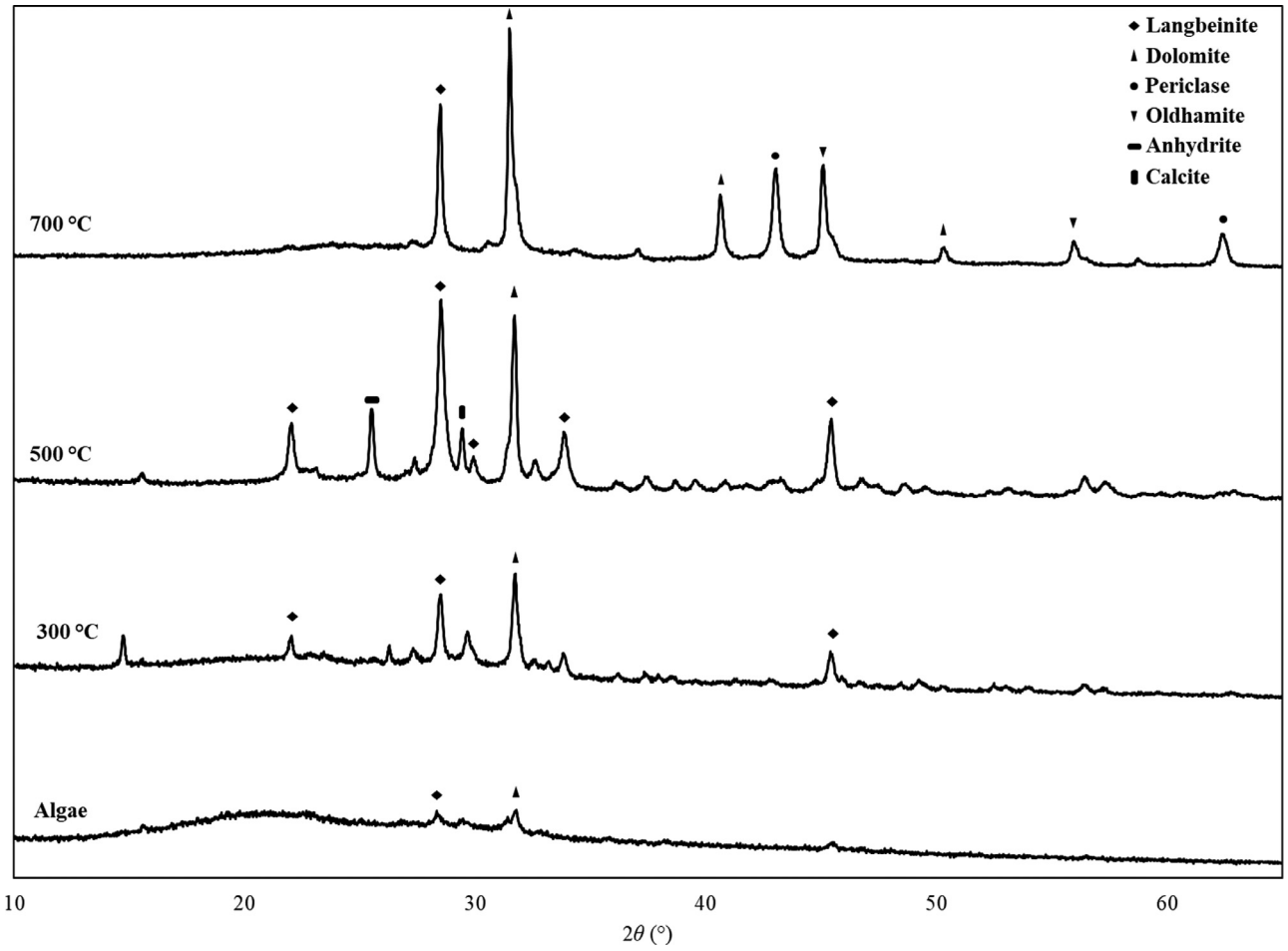

Fig. 2. XRD of MA (*Ulva Ohnoi*) and biochar produced at three different pyrolysis temperatures.

designated 2-theta angles, indicating the presence of certain minerals in the biochars. Especially, Langbeinite ($K_2Mg_2(SO_4)_3$) and dolomite ($CaMg(CO_3)_2$) were most prominent in all three biochar samples. At higher temperatures, minerals containing Mg i.e. periclase (MgO), Ca i.e. calcite ($CaCO_3$), and anhydrite ($CaSO_4$), or both Ca and Mg i.e. oldhamite ((Ca, Mg) S) appeared in the biochar samples. It is evident that with a rise in the pyrolysis temperature, the crystalline phases of calcite and dolomite became more prominent.

3.5. Phosphorus removal

3.5.1. Batch experiments for the removal of phosphorus

Fig. 3 demonstrates the results of batch experiments to understand the adsorptive removal of phosphorous. Biochar's adsorption capacity depends significantly on the pyrolytic temperature of MA. The adsorption capacity of dry algae and biochar produced at 300 °C (BC300) is very similar and less than 1 mg g^{-1}. There was an exponential increase of phosphorus adsorption capacity for biochar obtained at temperatures between 300 and 700 °C (Fig. 3). For biochars produced at 700 °C and 800 °C, the adsorption capacity was identical and stable at about 78 mg g^{-1}, which was four times more than the phosphorus adsorption capacity of biochar obtained at 600 °C (BC600). The higher adsorption capacity for these biochar samples can be ascribed to their exceptional textural properties, such as having higher SA and pore volume that allowed the adsorption of increased number of phosphorous species.

From these preliminary experiments and taking into consideration an economical perspective, biochar produced at 700 °C (BC700) was selected for further studies in terms of kinetics and isotherms and results are presented and discussed in the followed section.

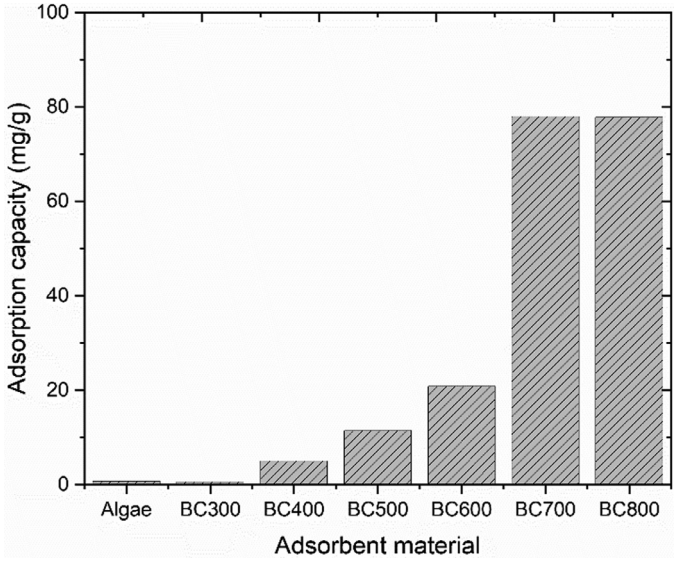

Fig. 3. Adsorption capacity of dry MA and MA derived biochar produced at different pyrolytic temperatures.

3.5.2. Adsorption kinetics

Table 2 summarises the results of kinetic studies and the associated model parameters. The mathematical modelling of the experimental data is presented in Fig. S5. Pseudo second-order model fits the

Table 2
Phosphorus adsorption kinetics for different models.

Kinetic model	Rate constant	Constant	R^2
Pseudo first-order	$k_1 = 0.52\ h^{-1}$	Q_e = 68.6 mg/g	0.96
Pseudo second-order	k_2 = 3.2 mg/(mg h)	Q_e = 92.6 mg/g	0.99
Intra-particle diffusion	k_{id} = 18.2 g/(mg $h^{1/2}$)	C = 8.1 mg/g	0.89
Elovich	a = 0.97	b = 0.05	0.95

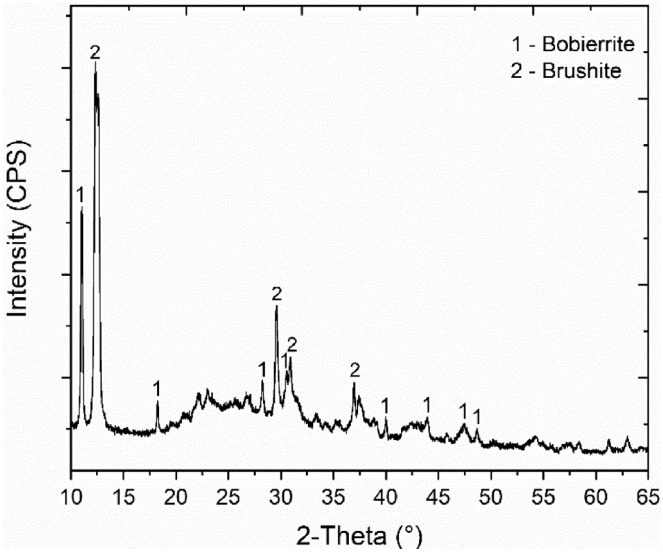

Fig. 4. XRD spectrum of the BC700 biochar after phosphorus adsorption experiments (1-Bobierrite and 2-Brushite).

data well (R^2=0.99) and the findings suggest that chemical adsorption is the major phosphorus adsorption mechanism with MA derived biochar produced at 700 °C, which can be explained by the complexation of phosphorus with certain abundant elements in the biochar such as calcium, magnesium and iron. Chemical adsorption can be confirmed by the XRD (Fig. 4) after phosphorus adsorption experiments, new peaks were available in the XRD spectrum of biochar, which match to brushite, commonly referred as calcium hydrogen phosphate dihydrate ($CaHPO_4 \cdot 2H_2O$), and bobierrite that is obtained from the reaction between magnesium ions and phosphate species ($Mg_3(PO_4)_2 \cdot 8H_2O$) – Eq. (17). Brushite is a thermodynamically stable phase formed from the reaction of Ca^{2+} with H_2PO^{4-} as described in Eq. (18).

$$3Mg^{2+} + 2PO_4^{3-} + 8H_2O \rightarrow Mg_3(PO_4)_2.8H_2O_{(s)} \quad (17)$$

$$Ca^{2+} + HPO_4^{2-} + 2H_2O \rightarrow CaHPO_4.2H_2O_{(s)} \quad (18)$$

3.5.3. Adsorption isotherms

The impact of phosphorus concentration on adsorption capacity of biochar can be observed in Fig. 5, which demonstrates an increase of adsorption capacity with the increase of adsorbate concentration up to a concentration of 400 mg/L, but then a significant decrease in the adsorption capacity for phosphorus concentrations above 500 mg/L was observed. These results are hard to be fitted with any isotherm model as desorption is not considered by these models. The potential explanation for this atypical relationship between adsorption capacity and concentration of adsorbate can also be found in Fig. 5 that includes the concentration of potassium, calcium and magnesium in solution.

As the concentration of phosphorus increases there is an increase on complexation of phosphorus with potassium, followed by solubility of potassium dihydrogen phosphate in the solution, then the overall adsorption of phosphorus on the biochar decreases. Solubility of calcium in the solution is lower than 1 mg/L for all phosphorus concentrations

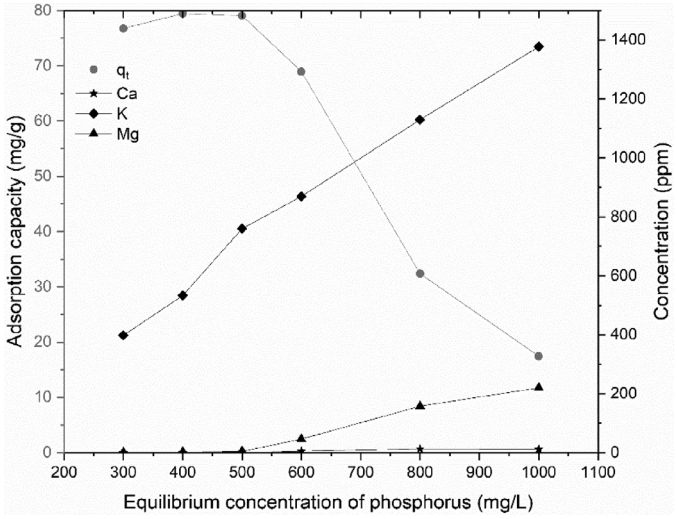

Fig. 5. Impact of phosphorus concentration on adsorption capacity of MA derived biochar and solubility of exchangeable cations concentration (K^+, Ca^{2+} and Mg^{2+}).

tested while the solubility of magnesium in the solution is also very low, reaching 10 mg/L in solutions with 1000 mg-P/L as can be observed in Fig. 5. The biochar produced from MA is rich in calcium, which is the main element for the high phosphorus adsorption capacity. However, the chemical composition of this biochar is complex and as well as rich in other inorganic species (magnesium and potassium) with high impact on phosphorus adsorption. In fact, potassium is the main inorganic responsible for a high desorption rate for concentration above 500 mg-P/L, which can be explained by the high solubility of potassium phosphate in water.

In P solution with a concentration above 500 mg-P/L, there is a clear competition between adsorption/desorption rates and solubility of phosphate compounds in solution. This will require further investigation to determine feasible conditions to maximize phosphorus adsorption by biochar naturally enriched with exchangeable elements and phosphorus. However, it is important to note that the adsorption capacity of the biochar produced in this study has a much higher adsorption capacity than the findings reported in literature (Table 3). Therefore, this study recommends the application of biochar derived from MA as a potential adsorbent for phosphate removal from domestic wastewater that contains less than 500 mg-P/L.

3.6. Techno-economic analysis

Results from techno-economic analysis for biochar production in a pilot scale plant (6t/day capacity) are reported in Table 4. The total biochar production cost in the pilot plant was estimated by adding the annual capital cost and annual fixed and variable operating costs, while biochar yield obtained at 700 °C (30.5%) was used to calculate the biochar production cost. The results revealed that one tonne of biochar could be produced at a cost of USD 710 in the pilot scale plant using MA feedstock. This unit cost could be reduced if the biochar yield is higher in the pyrolysis process. In addition to the biochar, other pyrolysis products such as bio-oil are also generated, which can be sold at a price of USD 410/tonne that is an additional revenue (Islam et al., 2011). Therefore, total unit biochar production can be further reduced from USD 710 to USD 485/tonne. However, it was observed that producing biochar using MA could be slightly expensive compared to other biomass feedstocks, which is mainly because of the cost associated with drying MA feedstock that contains high moisture content. This cost can be compensated by the high quality of biochar obtained from MA that achieved remarkable phosphorous adsorption.

Table 3
Phosphorus adsorption capacity by biochar produced from different biomasses.

Adsorbent	Initial Concentration (mg-P L^{-1})	Q (mg g^{-1})	Refs.
Ulva ohnoi biochar	500	78	This study
Biosolids biochar	500	16.4	Antunes et al. (2017b)
Ca-doped biosolids biochar	500	40	Antunes et al. (2018a)
Iron impregnated coir pith	1000	70.9	Krishnan and Haridas (2008)
Metal-loaded orange waste	1000	13.9	Biswas et al. (2007)
Fe(III)-treated Staphylococus xylosus biomass	1000	70.9	Aryal and Liakopoulou-Kyriakides (2011)
$Ca(OH)_2$-pretreated natural zeolite	200	7.6	Mitrogiannis et al. (2017)
Zirconium (IV) loaded cross-linked chitosan particles	300	71.7	Li et al. (2016)

Table 4
Techno-economic analysis for biochar production from MA feedstock in a pilot scale plant (6t/day).

Parameters used for cost analysis		Production cost (USD)	
Location, time, currency	Australia, 2021, USD	Base equipment cost	120,000
Annual operation time	7521 h	Fixed capital investment (FCI)	273,000
Maintenance	2.5% of FCI	Total capital required	313,950
Overheads	2% of FCI	Annual capital cost	58,848
Taxes and insurance	1.5% of FCI	Annual operating cost	
Other fixed operating costs	1% of FCI	Maintenance + overheads + taxes and insurance + other fixed operating cost	19,110
Labour cost[a]	15.26 USD/h (regular duty, 8 h/day), 6 labours	Total salary for employees	190,444
Feedstock cost	28 USD/ton	Feedstock	52,584
Electricity price[b]	0.17 USD/kWh (30 kW for pilot plant)	Electricity	38,311
General overheads	60% of total salaries	General overheads	114,266
Interest rate	10%	Total annual operating cost	414,715
Plant life	8 years	Total annual production cost	473,563
Biochar yield at 700 °C	30.5%	Unit production cost (US$/tonne)	710
By-products	Oil 375t/year, 400 USD/tonne	Revenue income	150,000
		Unit production cost after revenue (US$/tonne)	485

a-https://www.fairwork.gov.au/pay-and-wages/minimum-wages (AUD was converted into USD based on the current exchange rate). b-https://www.aer.gov.au/.

4. Conclusions

The study demonstrated the production of biochar from MA (*Ulva ohnoi*) under varying pyrolysis temperatures and its application for P removal from aqueous solution. Initial examination of TG analysis suggests that pyrolysis of *Ulva ohnoi* occurred in three stages, 50–150 °C: dehydration, 150–550 °C: thermal degradation of major structural components and 550–800 °C: thermal degradation of char and residues. The kinetics of pyrolysis indicated that the pyrolysis of *Ulva ohnoi* is a complex process with more than one reaction occurring simultaneously. The kinetics triplet evaluated in this study revealed pivotal information to design a reactor for the pyrolysis of similar feedstock. Macroalgae derived biochars produced at high temperatures resulted in an increase in the biochar's SA (178 m^2 g^{-1} at 800 °C), crystallization of calcite and hydrophobicity (lower H/C and O/C ratios). Additionally, amongst the biochars obtained at different temperatures, the biochar obtained at 700 °C achieved the highest P adsorption capacity (78 mg-P g^{-1} biochar). The best fitting kinetic model was pseudo second-order model, which indicates chemical adsorption as the main mechanism for P removal. Overall, this study suggests that the macroalgae derived biochar can serve as a low-cost adsorbent for the recovery of P from wastewaters, producing brushite which can be used as a slow release fertiliser in agriculture.

Declaration of Competing Interest

The authors declare that they have no known competing financial interests or personal relationships that could have appeared to influence the work reported in this paper.

Supplementary materials

Supplementary material associated with this article can be found, in the online version, at doi:10.1016/j.clcb.2022.100005.

References

Akahira, T., Sunose, T., 1971. Method of determining activation deterioration constant of electrical insulating materials. Res. Rep. Chiba Inst. Technol. (Sci. Technol.) 16(1971), 22–31.

Antoniou, N., Monlau, F., Sambusiti, C., Ficara, E., Barakat, A., Zabaniotou, A., 2019. Contribution to Circular Economy options of mixed agricultural wastes management: coupling anaerobic digestion with gasification for enhanced energy and material recovery. J. Clean. Prod. 209, 505–514.

Antunes, E., Jacob, M.V., Brodie, G., Schneider, P.A., 2017a. Silver removal from aqueous solution by biochar produced from biosolids via microwave pyrolysis. J. Environ. Manag. 203, 264–272.

Antunes, E., Jacob, M.V., Brodie, G., Schneider, P.A., 2018a. Isotherms, kinetics and mechanism analysis of phosphorus recovery from aqueous solution by calcium-rich biochar produced from biosolids via microwave pyrolysis. J. Environ. Chem. Eng. 6 (1), 395–403.

Antunes, E., Jacob, M.V., Brodie, G., Schneider, P.A., 2018b. Microwave pyrolysis of sewage biosolids: dielectric properties, microwave susceptor role and its impact on biochar properties. J. Anal. Appl. Pyrolysis 129, 93–100.

Antunes, E., Schumann, J., Brodie, G., Jacob, M.V., Schneider, P.A., 2017b. Biochar produced from biosolids using a single-mode microwave: characterisation and its potential for phosphorus removal. J. Environ. Manag. 196, 119–126.

Aryal, M., Liakopoulou-Kyriakides, M., 2011. Equilibrium, kinetics and thermodynamic studies on phosphate biosorption from aqueous solutions by Fe (III)-treated Staphylococus xylosus biomass: common ion effect. Colloids Surf. A Physicochem. Eng. Asp. 387 (1–3), 43–49.

Aziz, M., Oda, T., Kashiwagi, T., 2014. Advanced energy harvesting from macroalgae-innovative integration of drying, gasification and combined cycle. Energies 7 (12), 8217–8235.

Bach, Q.V., Chen, W.H., 2017. A comprehensive study on pyrolysis kinetics of microalgal biomass. Energy Convers. Manag. 131, 109–116.

Bheda, B., Shinde, M., Ghadge, R., Thorat, B., 2018. Drying of algae by various drying methods. In: Proceedings of the IDS 2018 21st International Drying Symposium. Editorial Universitat Politècnica de València, pp. 1791–1797.

Birner, R., 2018. Bioeconomy concepts. In: Lewandowski, I. (Ed.), Bioeconomy: Shaping the Transition to a Sustainable, Biobased Economy. Springer International Publishing, Cham, pp. 17–38.

Biswas, B.K., Inoue, K., Ghimire, K.N., Ohta, S., Harada, H., Ohto, K., Kawakita, H., 2007. The adsorption of phosphate from an aquatic environment using metal-loaded orange waste. J. Colloid Interface Sci. 312 (2), 214–223.

Ceylan, S., Kazan, D., 2015. Pyrolysis kinetics and thermal characteristics of microalgae Nannochloropsis oculata and Tetraselmis sp. Bioresour. Technol. 187, 1–5.

Ceylan, S., Topcu, Y., Ceylan, Z., 2014. Thermal behaviour and kinetics of alga Polysiphonia elongata biomass during pyrolysis. Bioresour. Technol. 171, 193–198.

Chen, W.H., Wu, Z.Y., Chang, J.S., 2014. Isothermal and non-isothermal torrefaction characteristics and kinetics of microalga Scenedesmus obliquus CNW-N. Bioresour. Technol. 155, 245–251.
Choi, Y.K., Kan, E., 2019. Effects of pyrolysis temperature on the physicochemical properties of alfalfa-derived biochar for the adsorption of bisphenol a and sulfamethoxazole in water. Chemosphere 218, 741–748.
Colantoni, A., Evic, N., Lord, R., Retschitzegger, S., Proto, A.R., Gallucci, F., Monarca, D., 2016. Characterization of biochars produced from pyrolysis of pelletized agricultural residues. Renew. Sustain. Energy Rev. 64, 187–194.
Dada, T.K., Sheehan, M., Murugavelh, S., Antunes, E., 2021. A review on catalytic pyrolysis for high-quality bio-oil production from biomass. Biomass Convers. Biorefin. 1–20.
Dandurand, J., Samouillan, V., Lacoste-Ferré, M.-H., Lacabanne, C., Bochicchio, B., Pepe, A., 2014. Conformational and thermal characterization of a synthetic peptidic fragment inspired from human tropoelastin: signature of the amyloid fibers. Pathol. Biol. 62 (2), 100–107.
Feizi, F., Reguyal, F., Antoniou, N., Zabaniotou, A., Sarmah, A.K., 2020. Environmental remediation in circular economy: end of life tyre magnetic pyrochars for adsorptive removal of pharmaceuticals from aqueous solution. Sci. Total Environ. 739, 139855.
Figueira, C.E., Moreira, P.F., Giudici, R., 2015. Thermogravimetric analysis of the gasification of microalgae Chlorella vulgaris. Bioresour. Technol. 198, 717–724.
Friedman, H.L., 1964. Kinetics of thermal degradation of char-forming plastics from thermogravimetry. Application to a phenolic plastic. J. Polym. Sci. Part C Polym. Symp. 183–195.
Fudholi, A., Othman, M., Ruslan, M., Yahya, M., Zaharim, A., Sopian, K., 2011. Design and testing of solar dryer for drying kinetics of seaweed in Malaysia. Recent Res. Geogr. Geol. Energy Environ. Biomed. 119–124.
Gai, C., Zhang, Y., Chen, W.T., Zhang, P., Dong, Y., 2013. Thermogravimetric and kinetic analysis of thermal decomposition characteristics of low-lipid microalgae. Bioresour. Technol. 150, 139–148.
Ghisellini, P., Cialani, C., Ulgiati, S., 2016. A review on circular economy: the expected transition to a balanced interplay of environmental and economic systems. J. Clean. Prod. 114, 11–32.
Giwa, A.S., Chang, F., Yuan, J., Ali, N., Guo, X., Wang, K., 2020. Evaluation of the potential beneficial pyrolyzed product yields from sewage sludge and bone waste disposal. Environ. Technol. Innov., 100784.
Hammond, L., Bai, L., Sheehan, M., Walker, C., 2018. Experimental analysis and diffusion modelling of solar drying of macroalgae-Oedogonium sp. Chem. Eng. Trans. 65, 427–432.
Hosseinizand, H., Sokhansanj, S., Lim, C.J., 2018. Studying the drying mechanism of microalgae Chlorella vulgaris and the optimum drying temperature to preserve quality characteristics. Drying Technol. 36 (9), 1049–1060.
Hu, Z., Chen, Z., Li, G., Chen, X., Hu, M., Laghari, M., Wang, X., Guo, D., 2015. Characteristics and kinetic studies of Hydrilla verticillata pyrolysis via thermogravimetric analysis. Bioresour. Technol. 194, 364–372.
Islam, M.R., Joardder, M.U., Hasan, S.M., Takai, K., Haniu, H., 2011. Feasibility study for thermal treatment of solid tire wastes in Bangladesh by using pyrolysis technology. Waste Manag 31 (9–10), 2142–2149.
Jung, K.-W., Jeong, T.U., Kang, H.J., Ahn, K.H., 2016. Characteristics of biochar derived from marine macroalgae and fabrication of granular biochar by entrapment in calcium-alginate beads for phosphate removal from aqueous solution. Bioresour. Technol. 211, 108–116.
Khawam, A., Flanagan, D.R., 2006. Solid-state kinetic models: basics and mathematical fundamentals. J. Phys. Chem. B 110 (35), 17315–17328.
Kim, B.S., Lee, H.W., Park, S.H., Baek, K., Jeon, J.K., Cho, H.J., Jung, S.C., Kim, S.C., Park, Y.K., 2016. Removal of Cu^{2+} by biochars derived from green macroalgae. Environ. Sci. Pollut. Res. 23 (2), 985–994.
Kim, J.E., Bhatia, S.K., Song, H.J., Yoo, E., Jeon, H.J., Yoon, J.Y., Yang, Y., Gurav, R., Yang, Y.H., Kim, H.J., 2020a. Adsorptive removal of tetracycline from aqueous solution by maple leaf-derived biochar. Bioresour. Technol., 123092.
Kim, J.E., Bhatia, S.K., Song, H.J., Yoo, E., Jeon, H.J., Yoon, J.Y., Yang, Y., Gurav, R., Yang, Y.H., Kim, H.J., Choi, Y.K., 2020b. Adsorptive removal of tetracycline from aqueous solution by maple leaf-derived biochar. Bioresour. Technol. 306, 123092.
Kim, K.H., Kim, J.-Y., Cho, T.S., Choi, J.W., 2012. Influence of pyrolysis temperature on physicochemical properties of biochar obtained from the fast pyrolysis of pitch pine (Pinus rigida). Bioresour. Technol. 118, 158–162.
Konda, N.V.S.N.M., Singh, S., Simmons, B.A., Klein-Marcuschamer, D., 2015. An Investigation on the Economic Feasibility of Macroalgae as a Potential Feedstock for Biorefineries. Bioenergy Res. 8 (3), 1046–1056.
Krishnan, K.A., Haridas, A., 2008. Removal of phosphate from aqueous solutions and sewage using natural and surface modified coir pith. J. Hazard. Mater. 152 (2), 527–535.
Li, J., Dai, J., Liu, G., Zhang, H., Gao, Z., Fu, J., He, Y., Huang, Y., 2016. Biochar from microwave pyrolysis of biomass: a review. Biomass Bioenergy 94, 228–244.
Lucaci, A.R., Bulgariu, D., Ahmad, I., Lisă, G., Mocanu, A.M., Bulgariu, L., 2019. Potential use of biochar from various waste biomass as biosorbent in Co (II) removal processes. Water (Basel) 11 (8), 1565.
Maurya, R., Ghosh, T., Saravaia, H., Paliwal, C., Ghosh, A., Mishra, S., 2016. Non-isothermal pyrolysis of de-oiled microalgal biomass: kinetics and evolved gas analysis. Bioresour. Technol. 221, 251–261.
Michalak, I., Baśladyńska, S., Mokrzycki, J., Rutkowski, P., 2019. Biochar from a freshwater macroalga as a potential biosorbent for wastewater treatment. Water (Basel) 11 (7), 1390.
Mishra, G., Bhaskar, T., 2014. Non isothermal model free kinetics for pyrolysis of rice straw. Bioresour. Technol. 169, 614–621.
Mitrogiannis, D., Psychoyou, M., Baziotis, I., Inglezakis, V.J., Koukouzas, N., Tsoukalas, N., Palles, D., Kamitsos, E., Oikonomou, G., Markou, G., 2017. Removal of phosphate from aqueous solutions by adsorption onto Ca (OH) 2 treated natural clinoptilolite. Chem. Eng. Journal 320, 510–522.
Muniz, M.A.P., dos Santos, M.N.F., da Costa, C.E.F., Morais, L., Lamarão, M.L.N., Ribeiro–Costa, R.M., Silva-Júnior, J.O.C., 2015. Physicochemical characterization, fatty acid composition, and thermal analysis of Bertholletia excelsa HBK oil. Pharmacogn. Mag. 11 (41), 147.
Nagarajan, D., Lee, D.J., Chen, C.Y., Chang, J.S., 2020. Resource recovery from wastewaters using microalgae-based approaches: a circular bioeconomy perspective. Bioresour. Technol. 302, 122817.
Nagarajan, S., Chou, S.K., Cao, S., Wu, C., Zhou, Z., 2013. An updated comprehensive techno-economic analysis of algae biodiesel. Bioresour. Technol. 145, 150–156.
Norouzi, O., Jafarian, S., Safari, F., Tavasoli, A., Nejati, B., 2016. Promotion of hydrogen-rich gas and phenolic-rich bio-oil production from green macroalgae Cladophora glomerata via pyrolysis over its bio-char. Bioresour. Technol. 219, 643–651.
Novais, S.V., Zenero, M.D.O., Barreto, M.S.C., Montes, C.R., Cerri, C.E.P., 2018. Phosphorus removal from eutrophic water using modified biochar. Sci. Total Environ. 633, 825–835.
Raheem, A., Prinsen, P., Vuppaladadiyam, A.K., Zhao, M., Luque, R., 2018. A review on sustainable microalgae based biofuel and bioenergy production: recent developments. J. Clean. Prod. 181, 42–59.
Sanchez-Silva, L., López-González, D., Garcia-Minguillan, A., Valverde, J., 2013. Pyrolysis, combustion and gasification characteristics of Nannochloropsis gaditana microalgae. Bioresour. Technol. 130, 321–331.
Sitepu, E.K., Corbin, K., Luo, X., Pye, S.J., Tang, Y., Leterme, S.C., Heimann, K., Raston, C.L., Zhang, W., 2018a. Vortex fluidic mediated direct transesterification of wet microalgae biomass to biodiesel. Bioresour. Technol. 266, 488–497.
Sitepu, E.K., Jones, D.B., Tang, Y., Leterme, S.C., Heimann, K., Zhang, W., Raston, C.L., 2018b. Continuous flow biodiesel production from wet microalgae using a hybrid thin film microfluidic platform. Chem. Commun. 54 (85), 12085–12088.
Soltangheisi, A., Withers, P.J., Pavinato, P.S., Cherubin, M.R., Rossetto, R., Do Carmo, J.B., da Rocha, G.C., Martinelli, L.A., 2019. Improving phosphorus sustainability of sugarcane production in Brazil. GCB Bioenergy 11 (12), 1444–1455.
Son, E.B., Poo, K.M., Chang, J.S., Chae, K.J., 2018. Heavy metal removal from aqueous solutions using engineered magnetic biochars derived from waste marine macro-algal biomass. Sci. Total Environ. 615, 161–168.
Söyler, N., Goldfarb, J.L., Ceylan, S., Saçan, M.T., 2017. Renewable fuels from pyrolysis of Dunaliella tertiolecta: an alternative approach to biochemical conversions of microalgae. Energy 120, 907–914.
Sun, D., Hale, L., Kar, G., Soolanayakanahally, R., Adl, S., 2018. Phosphorus recovery and reuse by pyrolysis: applications for agriculture and environment. Chemosphere 194, 682–691.
Ubando, A.T., Felix, C.B., Chen, W.H., 2020. Biorefineries in circular bioeconomy: a comprehensive review. Bioresour. Technol. 299, 122585.
Veni, D.K., Kannan, P., Edison, T.N.J.I., Senthilkumar, A., 2017. Biochar from green waste for phosphate removal with subsequent disposal. Waste Manag. 68, 752–759.
Vuppaladadiyam, A.K., Liu, H., Zhao, M., Soomro, A.F., Memon, M.Z., Dupont, V., 2019a. Thermogravimetric and kinetic analysis to discern synergy during the co-pyrolysis of microalgae and swine manure digestate. Biotechnol. Biofuels 12 (1), 170.
Vuppaladadiyam, A.K., Zhao, M., Memon, M.Z., Soomro, A.F., 2019b. Microalgae as a renewable fuel resource: a comparative study on the thermogravimetric and kinetic behavior of four microalgae. Sustain. Energy Fuels 3 (5), 1283–1296.
Walker, C., Cole, A., Antunes, E., Sheehan, M., 2020. Equilibrium Moisture and Drying Kinetics Modelling of Macroalgae Species Ulva ohnoi and Oedogonium intermedium. Clean. Technol. 2 (2), 225–239.
Wnetrzak, R., Kwapinski, W., Peters, K., Sommer, S.G., Jensen, L.S., Leahy, J., 2013. The influence of the pig manure separation system on the energy production potentials. Bioresour. Technol. 136, 502–508.
Yuan, Z., Jiang, S., Sheng, H., Liu, X., Hua, H., Liu, X., Zhang, Y., 2018. Human perturbation of the global phosphorus cycle: changes and consequences. Environ. Sci. Technol. 52 (5), 2438–2450.
Zhang, G., Guo, X., Zhao, Z., He, Q., Wang, S., Zhu, Y., Yan, Y., Liu, X., Sun, K., Zhao, Y., 2016. Effects of biochars on the availability of heavy metals to ryegrass in an alkaline contaminated soil. Environ. Pollut. 218, 513–522.
Zhao, M., Raheem, A., Memon, Z.M., Vuppaladadiyam, A.K., Ji, G., 2019. Iso-conversional kinetics of low-lipid micro-algae gasification by air. J. Clean. Prod. 207, 618–629.
Zheng, H., Wang, Z., Zhao, J., Herbert, S., Xing, B., 2013. Sorption of antibiotic sulfamethoxazole varies with biochars produced at different temperatures. Environ. Pollut. 181, 60–67.